Final state effects in photoemission studies of Fermi surfaces

2007 J. Phys.: Condens. Matter 19 355001

(http://iopscience.iop.org/0953-8984/19/35/355001)

IOP PUBLISHING JOURNAL OF PHYSICS: CONDENSED MATTER

J. Phys.: Condens. Matter **19** (2007) 355001 (14pp) doi:10.1088/0953-8984/19/35/355001

Final state effects in photoemission studies of Fermi surfaces

Richard L Kurtz[1,3], **Dana A Browne**[1] **and Gary J Mankey**[2]

[1] Department of Physics and Astronomy, Louisiana State University, Baton Rouge, LA 70808, USA
[2] Department of Physics and Astronomy, University of Alabama, Tuscaloosa, Tuscaloosa, AL 35487, USA

E-mail: rlkurtz@lsu.edu

Received 15 March 2007, in final form 6 August 2007
Published 20 August 2007
Online at stacks.iop.org/JPhysCM/19/355001

Abstract

Photoelectron spectroscopy is one of the most important methods for extracting information about the Fermi surface (FS) of materials. An electron photoexcited from the FS is emitted from the crystal conserving the parallel momentum, $k_{\|}$, while the perpendicular momentum $k_{\perp}$ is reduced due to the surface potential barrier. A simple interpretation of the process assumes the final state is free-electron-like allowing one to 'map' the detected photoelectron back to its initial k momentum. There are multiple final state effects that can complicate the interpretation of photoelectron data and these effects are reviewed here. These can involve both energy and k broadening, which can give rise to shadow or ghost FS contours, scattering and final state diffraction effects that modify intensities, and matrix element effects which reflect the symmetries of the states involved and can be highly dependent on photon polarization. These matrix elements result in contours of photoelectron intensity that follow the dispersion in k-space of the initial state, the FS, and the final state. Locations where intensities go to zero due to matrix element and symmetry effects can result in gaps where FS contours 'disappear'. Recognition that these effects can play a significant role in determining the measured angular distributions is crucial in developing an informed model of where the FS contours actually lie in relation to measured intensity contours.

1. Introduction

The electrons at the Fermi surface determine the transport properties of materials. Photoelectron spectroscopy is one of the most important experimental methods used to extract information on shape of the Fermi surface (FS). Photoemission can be used to probe the FS of materials in 1, 2, and 3D, in a broad range of temperatures allowing for phase transitions

[3] Author to whom any correspondence should be addressed.

to be studied, and does not require the extremely perfect crystals needed for de Haas–van Alphen or other magneto-oscillatory probes. Ideally, one is interested in extracting the contour of the FS from the photoemission intensity distributions measured as a function of electron detection angle and photon energy. These detected photoelectrons arise from a matrix element that couples the initial state, the FS, with those final excited states that then couple efficiently with the plane waves that exit the crystal. This process involves several effects that can modify the photoemission angular distribution and can complicate the direct interpretation of the experimental data. In this paper, we review several of these effects and expand on the photon polarization dependence of the matrix elements. Polarization effects on the measured angular distributions are highly dependent on the experimental geometry and it is important to specify this geometry in detail in order to properly interpret synchrotron-based FS studies.

There are many excellent reviews of the principles of photoemission [1, 2], and the techniques for using it to extract the electronic band structure $\varepsilon(\mathbf{k})$, the electron binding energies, ε, as a function of their wavevector $\mathbf{k}$ within the Brillouin zone. Here, we only mention the elements of photoemission key to the issues discussed below. The differential matrix element for photoelectron excitation $\mathrm{d}\sigma$, per solid angle $\mathrm{d}\Omega$ is, under the approximation of a slowly varying vector potential, $\mathbf{A}$, given by

$$\frac{\mathrm{d}\sigma}{\mathrm{d}\Omega} \sim |\langle f|\mathbf{A}\cdot\mathbf{p}|i\rangle|^2 \tag{1}$$

where $\mathbf{p}$ is the momentum operator and $|i\rangle$ and $\langle f|$ are the initial and final state wavefunctions. The photoelectron in the final state $\langle f|$ must then couple to the plane waves that efficiently transport the electron into vacuum. In crossing the surface/vacuum potential barrier, the parallel component of the momentum, $k_{\|}$, is conserved while $k_{\perp}$ is not, creating uncertainty in the initial momentum through this change due to the inner potential. The transport of the excited plane waves to the surface can include other extrinsic effects such as diffraction that can modify intensities, and result in intensity in new directions. Other uncertainties also can come into play in the photoemission event, including broadening in ε and in $\mathbf{k}$ in either or both the initial and final states. The momentum matrix element also plays a key role in the sense that it couples the symmetries of the initial and final states, dictating the locations in $\mathbf{k}$ where transitions are possible. Finally, the intensities from this complex matrix element are dependent on the photon polarization through the vector potential, $\mathbf{A}$. This polarization is controlled by the experimental geometry and the matrix elements for differing photoelectron emission directions relative to $\mathbf{A}$ will in general differ, even for transitions involving the same initial and final states.

It is possible to simplify many of these effects, for example by working in purely normal emission, or to measure bands and their FS crossings only along axes of high symmetry. In these cases, symmetry considerations can provide straightforward interpretations. In more complete mappings of FS crossings, we are interested in following the dispersion of the FS structure through the full dimension of relevance, whether it is the 2D or 3D reciprocal space. This means that photoemission events in regions of low symmetry are of interest, and more detailed modeling of the photoemission matrix elements through equation (1) are needed.

Most of the work on quantitative photoemission and Fermi surface determination has involved either simple $3d$ transition metals such as Cu or Ni, or high temperature superconductors such as Bi2212 where there is intense interest in the understanding the fine details of the FS. Our examples will involve these materials.

2. Character of the initial and final states

A general discussion of the limitations of photoemission in providing quantitative electronic band mapping has been provided by Strocov [3]. Central in the problem of relating features in

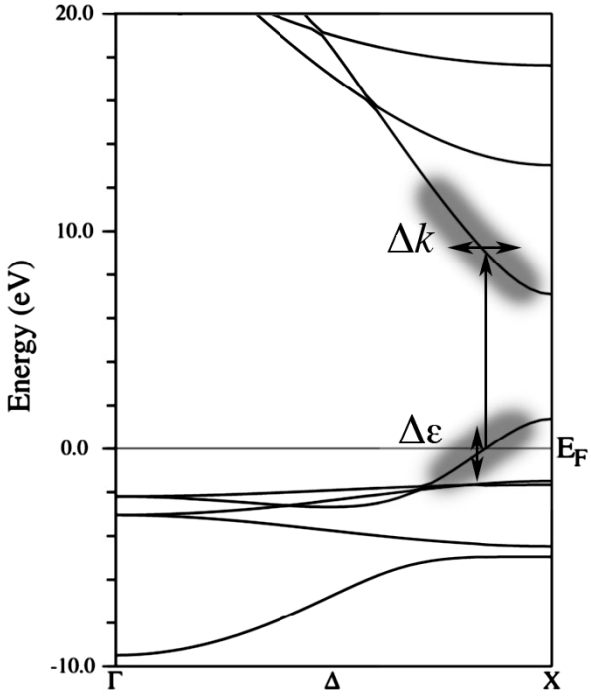

Figure 1. Mechanisms that produce a spread in ε and in k create uncertainties in relating spectral features to the initial state band structure, $\varepsilon(\mathbf{k})$. For example, normal emission from the (001) face of an fcc lattice involves $\mathbf{k}$-vectors mapped along the Δ symmetry line that are purely $k_\perp$.

the spectra to the electronic band structure, $\varepsilon(\mathbf{k})$, is the extent that the initial state momentum, $\mathbf{k}^{\mathrm{i}}$, and in particular, $k_\perp^{\mathrm{i}}$, can be determined precisely and unambiguously. The transition from the initial occupied state to the final state involves uncertainty in both ε and in $\mathbf{k}$ as illustrated in figure 1 and the origins of these uncertainties differ for the initial and the final states.

These uncertainties give rise to linewidths in the measured spectra with contributions from both the hole left behind, as well as the electron in the excited state. In the 3d electron bands of Cu, this has been related to the lifetimes of the electron and hole as well as the group velocities of the bands involved [4].

In the initial state, the wavevector $\mathbf{k}_{\mathrm{i}}$ in the bulk is well defined (Δk_{i} is small) but the energy ε as measured in photoemission has an intrinsic linewidth $\Delta\varepsilon_{\mathrm{i}}$ that arises due to the finite lifetime, τ_{h}, of the hole left behind in the excitation process where $\Delta\varepsilon_{\mathrm{i}} = \hbar/\tau_{\mathrm{h}}$. In Cu, for example, these hole lifetimes give rise to energy widths ranging from 20 meV to nearly 500 meV, depending on which excitation is involved [4, 5]. Although the surface termination breaks the symmetry of the bulk, the screening is so rapid in metals that the bulk-like nature of the initial state wavevector is retained and the smearing of $\mathbf{k}_{\mathrm{i}}$ is small. An example that illustrates the coupling of bulk-like $\mathbf{k}$ dispersion to even the topmost monolayer of atoms is the case for a monolayer of Ni on Cu(100) [6]. In that case bulk-like ARPES Ni spectra, including the appropriate $k_\perp$ dispersion, was found in the epitaxial Ni monolayer due to coupling of the Cu substrate Bloch periodicity to the surface.

The final state of the photoemission process is responsible for many more of the difficulties involved in relating measured spectra to the initial state band structure, $\varepsilon(\mathbf{k})$. Intrinsic smearing in both ε and $\mathbf{k}$ can occur and the final excited state bands $E_{\mathrm{f}}(\mathbf{k})$ (where the E denotes

the *excited*-state energies), actually differ measurably from the final state bands $\varepsilon_f(\mathbf{k})$ in the *absence* of the excitation [7]. One method to gain information on the final states is to measure the time-reversed LEED states through very low energy electron diffraction (VLEED) [7]. Although this differs from the photoemission final state due to the lack of the hole created in the excitation, it can provide valuable information on the differences between the excited and ground state final state bands, and the estimates for the electron–hole interaction energies, E_{e-h}, are less than 100 meV for typical experiments [8]. Furthermore, as it is a measured diffraction event, it provides information on the coupling of the vacuum plane waves with the internal final state Bloch waves that are responsible for the photocurrent [9]. This has been shown to give measurable differences between the experimental and theoretical final states and improves agreement between experiment and the results of density functional theory [9].

Energy broadening can result from the finite electron lifetime giving a width $\Delta\varepsilon_f = \hbar/\tau_e$ and this can play a role in instruments with low energy resolution (such as the display analyzer discussed below). Broadening of $k_\perp$ results in larger discrepancies with the predicted ground state final states $\varepsilon_f(\mathbf{k})$. The broadening of these final states is due to inelastic absorption related to the electron lifetime as well as elastic scattering, and these result in a damping of the final state wavefunction [3]. These effects are expressed as the self-energy $\Sigma = E - \varepsilon$, the energy difference between the final state energies in the excited versus ground state conditions. The broadening and corresponding final state lifetimes, $\hbar/\tau = 2\,\mathrm{Im}\,\Sigma$, depend on the energy of the final states, and can change as the Im Σ varies. In Cu, the hole lifetimes ranged from 1.25 to 1.75 eV for final states between 10 and 14 eV. For Bi2212 the lifetime broadening was found to range from 0.25 eV for final states located at $E_f = 5$ eV, to 3 eV at $E_f = 45$ eV and the change was attributed to two plasmons that develop in that energy range [8].

These observations indicate that the final state widths that need to be considered in an excitation may not simply be intrinsic but may be influenced by collective excitations. As we discuss below, regardless the source of the broadening, it is essential that final states within a non-negligible width be considered in relating a predicted angular distribution with those that are experimentally measured.

3. Fermi surface impostors: ghosts and shadows

The E and $\mathbf{k}$ broadening gives rise to several effects that can appear to give Fermi surface crossings. For $\mathbf{k}$ broadening, a width in $k_\perp$ gives spectra which have a finite energy width, despite the fact that the initial energy $\varepsilon_i(\mathbf{k})$ may be well defined. The $k_\perp$ width of the final state allows transitions to occur at $k_\perp$ where the initial state has dispersed above E_F. Although this is just a tail of the original allowed transition, it results in measurable intensity at E_F in a peak that appears to be fixed in energy. This peak is then mapped to disperse up to the point where the state is above E_F and then remains at a fixed energy through k-space. This is seen in the study of the band structure of Na [10] and has been seen in other systems as well. In some systems such as $NbSe_2$ the non-dispersive 'ghost' intensity can be so large as to prevent the mapping of less intense features of the FS [11].

An extrinsic effect that produces a 'shadow' Fermi surface involves photoelectron diffraction producing intensity in regions that would not normally involve a transition. For Bi2212, a VLEED study showed that a hidden c(2 × 2) diffraction pattern can be seen below 25 eV along ΓY but disappears at higher final state energies [8]. This produces intensity at E_F as a so-called shadow FS, and is also found to appear elsewhere within the Brillouin zone, at the M point. In this case, being an extrinsic effect, it can be avoided by tuning the experiment to involve higher energy final states by using higher energy photons.

4. Matrix element effects

Although there is continuing interest in understanding the fundamentals of angle-resolved photoelectron spectroscopy (ARPES), a large amount of work has been motivated by the interest in understanding the Fermi surfaces of high temperature superconductors. The Fermi surface is key in understanding transport properties and its structure, and subtle interactions with it are important in the origin of superconductivity. Since understanding the subtleties is so critical, it is crucial that the origins of the photoemission event are well understood. To this end, several groups actively work to understand the details of the initial and final states in (1) and in understanding the matrix elements between them.

Bi2212 is one of the more studied high T_cs, in part because of the availability of high quality crystals and their easier cleavage in vacuum resulting in higher quality data. For this reason, a significant body of theoretical work is aimed at understanding its FS.

Because the matrix elements between the initial and final states in (1) involve states of different symmetries that disperse in energy, the photoelectron spectra obtained from the FS of Bi2212 are not simply contours of uniform intensity at the loci of k-space points where bands cross E_F. The matrix elements introduce significant angular dependence in the photoemitted intensity. Bansil has carried out first-principles (LDA) calculations for photoemission from Bi2212 that include the initial and final states as well as corrections for multiple scattering in the presence of the surface [12]. In that study they found that the intensity at the FS attributed to the CuO_2 planes was highly anisotropic as a function of k_x and k_y and that there were significant departures from the one-particle spectral density $\varepsilon(\mathbf{k}_F)$ [12].

In a further study, the same group found that these matrix elements varied significantly as a function of the incident photon energy, $h\nu$, and that different transitions varied significantly from one another [13]. A key aspect of these results is the recognition that different aspects of the electronic structure are highlighted differently as a function of $h\nu$. In fact, they find that for $h\nu$ below 25 eV, only the O $2p$ component of the CuO_2 planes is sampled through $p \rightarrow d$ transitions despite the admixture of some Cu in that state [14]. Only at higher energies are the Cu states sampled. These results also suggest that by tuning the photon energy, one can establish the conditions to enhance transitions from one specific component of the Fermi surface. For multicomponent materials like the high T_cs this allows one to focus either on the O $2p$ or the Cu $3d$ contributions to the FS. In other materials, tuning $h\nu$ has the potential to establish transitions from separate portions of the FS. These observations also underscore the need for a theoretical analysis to accompany experimental data for the most accurate interpretation of the meaning of the results.

4.1. Polarization dependence

Many of the angle-scanned studies of FS topology using ARPES use resonance lamps providing unpolarized ultraviolet light [15]. This has the advantage that all of the possible transitions at that energy are sampled. On the other hand, those studies that aim at probing the 3D topology of the FS, utilize synchrotron radiation in order to be able to study the FS by varying $k_\perp$ as well as scanning over $k_\parallel$. This establishes a key difference in these measurements. The synchrotron radiation is linearly polarized and this leads to a photoelectron spectrum where the direction of the incident polarization relative to the Brillouin zone, as well as the direction of emission of the electron excited from the FS need to be taken into consideration when computing a matrix element.

In the following pages, we will review the issues that arise with polarized light and the influence that the experimental geometry has on the measured photoelectron spectra. We

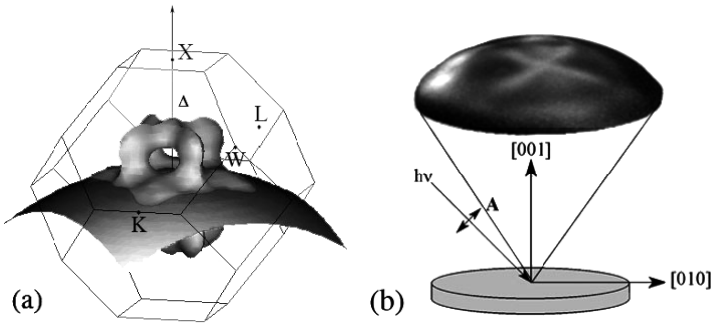

Figure 2. (a) Photoemission occurs where the final state intersects occupied states within the Brillouin zone. (b) In a display analyzer, the ARPES intensities are detected in a single image.

will show that the matrix elements calculated with a specific experimental geometry vary dramatically as this geometry changes. We will also compare the measured photoelectron angular distributions with first-principles calculations to assess the origin of the structures measured in terms of the contributions from the initial and final states.

The data that we present here were acquired at the LSU Center for Advanced Microstructures and Devices (CAMD) synchrotron light source using an ellipsoidal mirror analyzer (EMA) on the plane-grating monochromator (PGM) [16–18]. This is a display-type electron energy analyzer that accepts electrons in a large solid angle and its operation has been described in detail elsewhere [18]. The energy resolution is fixed at ∼0.25 eV with the instrument operated in a constant pass energy mode.

Figure 2(a) shows a Fermi surface within an fcc Brillouin zone with a section of the shaded plane-wave (spherical) final state. This sphere is centered on Γ in the BZ below that shown, and its radius is appropriate for sampling near the bulk Γ-point of Cu or Ni at $h\nu = 45$ eV. The loci of points of the intersection of this final state surface with the occupied states of the FS gives the locations within k-space where transitions can occur. Figure 2(b) schematically shows the origin of data in a display-type analyzer image. Electrons emitted in a cone defined by the detector's angular acceptance are energy analyzed, and their intensities are collected over a range of emission angles. In the data shown here, p-polarized photons, are incident on the crystal at an angle of 45° so that non-zero A_x and A_z components provide the excitations.

The radius of the final state sphere in figure 2(a) depends on the electron kinetic energy, which in turn, depends on the photon energy used through the relations detailed in several reviews of photoemission [1, 2]. In normal emission from the Fermi surface of an fcc (001) surface, for example, the Γ–X direction, or the Δ line in the bulk Brillouin zone, will be probed as the photon energy is varied. For other combinations of photon energy and emission angle (or surface orientations), one can access other high symmetry points as labeled in figure 2(a) [1, 2]. It should be noted that this 3D **k**-space band mapping is distinct from the measurement of 2D surface electronic structure where dispersion is denoted by $\bar{\Gamma}$–$\bar{\mathrm{M}}$, for example.

There are several key aspects of this experimental geometry that are important in determining the emission patterns presented below. First, polarized light with components both perpendicular and parallel to the surface are involved so that by rotating the crystal azimuthally (around the surface normal) all transitions that can be stimulated, and which are compatible with the directions of the electron detection will be seen. The plane in which the light is incident is critical in determining the patterns, as symmetry selection rules govern emission not only in that plane, but in the other azimuthal directions as well. Second, the patterns that

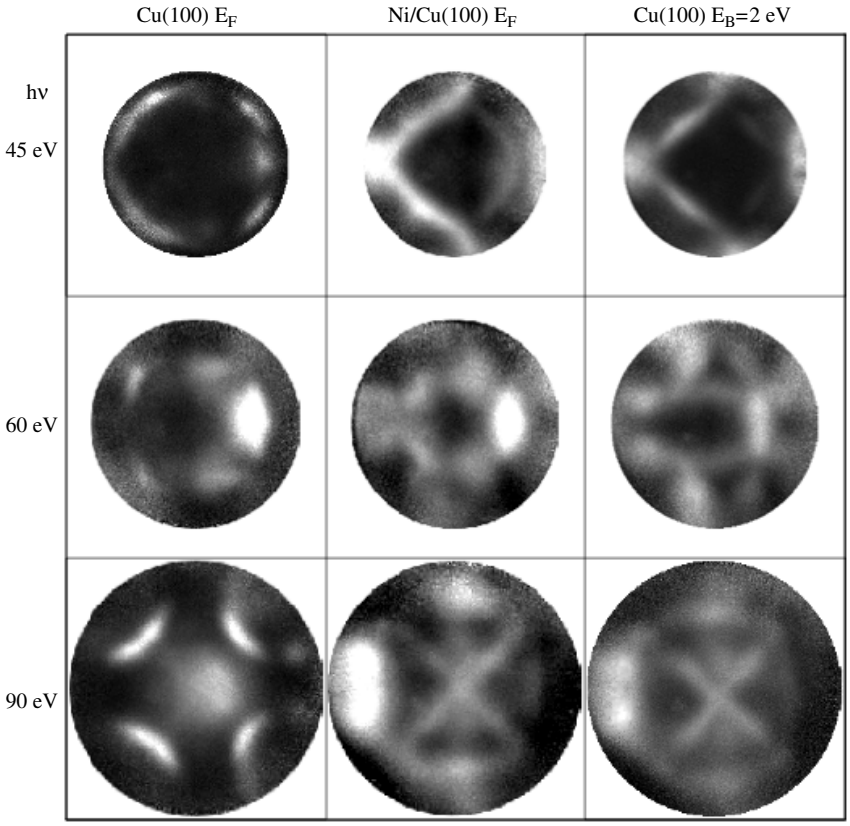

Figure 3. Measured ARPES from the Fermi levels of Cu(001), 1.2 ML Ni/Cu(001), where $E_B = 0$ eV, and from Cu(001) at a binding energy of 2 eV at photon energies of 45, 60, and 90 eV. Synchrotron light is polarized in the horizontal plane, the [010], at 45° from the vertical. Higher intensities are brighter.

are observed allow one to view all of the potential combinations of incident crystalline plane, polarization direction, and emission angle within the acceptance of the instrument. This is unlike most configurations with conventional hemispherical analyzers that measure spectra at a single fixed angle relative to the incident photon direction and polarization. In order to vary $k_\parallel$ in those instruments it is necessary to rotate the sample and this continuously changes the incident polarization direction relative to the crystalline axes.

Examples of the data from an ARPES measurement using a display analyzer are shown in figure 3. In that figure, data from the Fermi surface of Cu(001), the Fermi surface of 1.2 ML Ni/Cu(001) and the 3d electron bands at $E_i = -2$ eV in Cu(001) are shown using photons of energies 45, 60, and 90 eV. The Cu(001) data at 90 eV (figure 3, lower left) show four slices into the bodies of the Fermi surfaces in adjacent Brillouin zones, while the lower photon energy data show the polarization dependence of the matrix elements for the states at E_F. We have shown previously that the Ni data from the 1.2 ML Ni/Cu(001) are essentially identical to that from single-crystal Ni(001). Note the similarity in the data between the Ni data from E_F and the Cu data at -2 eV binding energy. These are the same initial bands, the only difference being the higher binding energy of the Cu due to the greater band filling relative to Ni. In part this is also due to the very similar lattice constants of the two materials.

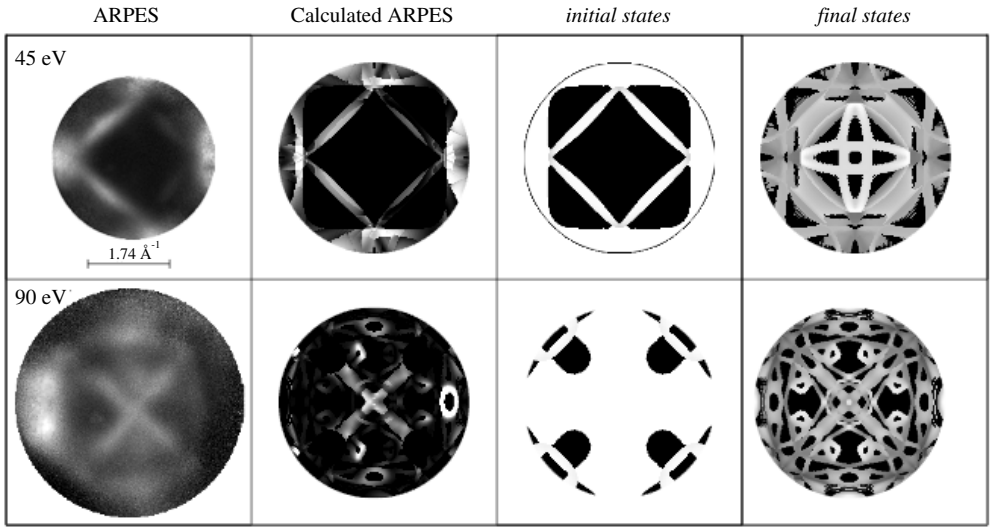

Figure 4. ARPES from Cu(100) at a binding energy of 2 eV at photon energies of 45 and 90 eV (left). Higher intensity is brighter. The calculated ARPES are shown as well as the initial and final states involved in producing the matrix elements.

The images are shown as projections of $k_\parallel$ so that the Δ line (along Γ–X) is crossed by the center of each image. The $k_\parallel$ dimension of each image also varies with $h\nu$ since the fixed acceptance angle of the instrument accepts a larger slice at higher energy. At 90 eV the images are approximately 4.9 Å^{-1} across while they are approximately 3.5 Å^{-1} across at 45 eV. As a function of photon energy, the center of the 45 eV image is $\sim$16% of $(2\pi/a)$ above Γ and the center of the 90 eV image is approximately $\sim$9%$(2\pi/a)$ below the X point.

There are several important aspects that one can immediately recognize from these images. First, there is a left–right asymmetry due to the orientation of the polarization relative to the surface in the horizontal plane. This asymmetry dramatically alters the intensity distributions for electrons emitted perpendicular to the **A** compared to those emitted along it. This shows that a photoemission measurement made in one 'irreducible wedge' of the surface Brillouin zone is not equivalent to that made in another, for the polarization orientation shown here. This also shows that a detailed understanding of the experimental geometry is needed to properly interpret the polarization dependence, particularly if the crystal is rotated to vary $k_\parallel$ in a manner that changes the incident polarization relative to the surface.

The second point is that the angular distributions vary dramatically with incident photon energy. This shows the $k_\perp$ dependence of ARPES as one slices through various parts of the Brillouin zone. It is often stated that by stacking a series of these images, one can then assemble a 'bulk 3D' Fermi surface. As discussed below, the matrix element dependences complicate such a simple interpretation.

The case of the 1.2 ML of Ni/Cu(100) is especially interesting since it implies that, rather than looking like a 2D film of atomic Ni, the Ni exhibits what appears to be a bulk-like Fermi surface. The angular distributions change with photon energy and, as mentioned, look like the Cu 3d states that are found at -2 eV. From the discussion of the origin of the Cu pattern given below, we will conclude that the 45 eV 1.2 ML Ni/Cu(100) data reflects the Fermi surface, or the initial state, while the 90 eV data reflect the structure of the final states, and *not* the Fermi surface dispersion of Ni/Cu(100).

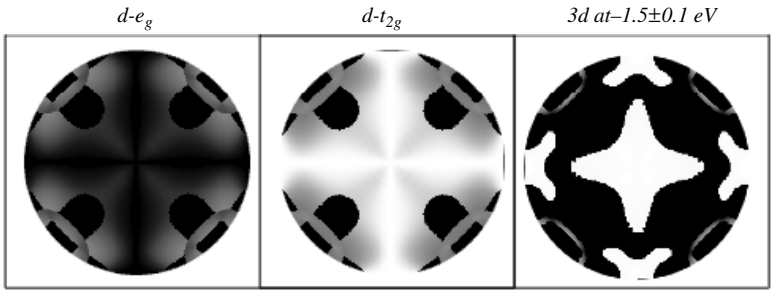

Figure 5. DOS of the d-e_g and d-t_{2g} initial states at -1.5 ± 0.25 eV sampled by 90 eV photons. On the right are the same states with a ± 0.1 eV window.

In figure 4, we present the angular distributions from Cu(100) measured at -2 eV binding energy using photons at 45 and 90 eV. In addition, we present a predicted ARPES image along with the initial and final states involved in the transition. The data were taken with a 'display' analyzer that has a constant acceptance angle so that the range of $k_\parallel$ sampled changes with photon energy. The size of the data image reflects this change while the calculations display a fixed $k_\parallel$ range that spans a cross-section of the 3D Brillouin zone.

The calculations were performed with the WIEN2K code [19] using the GGA of Perdew, Burke, and Ernzerhof [20]. Local s, p, and d orbitals were added to improve the quality of the final states. The ARPES angular distributions were obtained by calculating the matrix elements assuming an inner potential of 9 eV; the results were qualitatively insensitive to the value used within ± 1 eV. The initial states at -1.5 eV were used rather than -2 eV and this is consistent with the fact that density functional methods incorrectly underestimate the locations of the d bands, as previously noted [21, 22].

The ARPES 'image' was computed by taking the complex matrix elements computed at each k-point, the sphere in figure 2(a), dotted into the vector potential, following equation (1). The energy of the initial state strongly affected the structures calculated in the ARPES, a shift of 0.2 eV produced a computed ARPES that was a noticeably poorer match to the experimental data. An initial state lifetime, giving rise to an energy broadening of $\Delta\varepsilon_i = \pm 0.25$ eV was used. The self-energy of the final states gives rise to a lifetime broadening of $2\,\mathrm{Im}\,\Sigma$ and a value of ± 1.5 eV was used. The initial state broadening did not impact the structure of the calculated ARPES, it only affected how broad the computed intensity features were. It is much more important to account for the final state self-energy, since the dispersion and number of bands involved only produced sharp loci in k for allowed transitions at lower final state widths. Note that no other effects are provided for in these computations, such as surface effects.

In the right two columns of figure 4 we show the initial states ± 0.25 eV and the final states ± 1.5 eV that are involved at each photon energy. Note the density of states is given by the intensity within the circles with white being a high DOS and dark being low. At 45 eV, the diamond in the center is composed equally of d-e_g and d-t_{2g} while the states at the outer edges are mostly d-t_{2g}. The final states at 45 eV include states with p, d, and f character angular momentum but the transitions are located mostly on the f states. The predicted angular distribution matches the measured ARPES pattern, reflecting the shape of the initial state.

The situation changes when we look at the region of the BZ sampled by 90 eV photons. The structure of the predicted pattern matches well with the ARPES but looks unlike the contour of the initial state. The initial state DOS again consists of d-e_g and d-t_{2g} states but in this region of the BZ the d-t_{2g} states dominate as shown in figure 5. For reference, if one decreases the

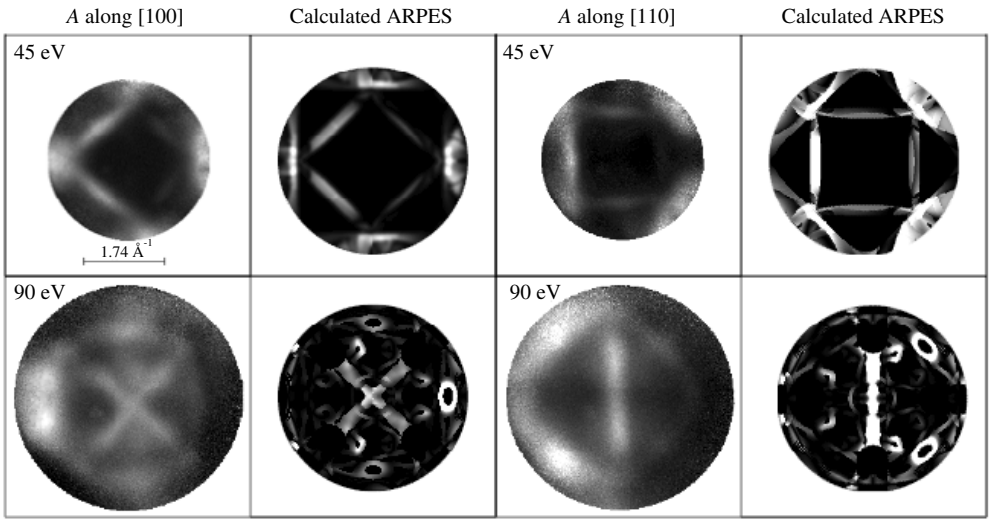

Figure 6. ARPES from Cu(001) at 2 eV binding energy using $h\nu = 45$ and 90 eV. The photon polarization is 45° relative to the surface normal with $\boldsymbol{A}$ either along the [100] or [110] azimuths; this change was accomplished by rotating the sample about its normal.

energy window on these initial states to ±0.1 eV, the pattern of states shrinks to that on the right in figure 5. None of these structures look like the 'X' seen in the data in figure 4. On the other hand when one compares the structure in the final states, a clear 'X' is seen in the f angular momentum components of the final state. This means that the contour of intensities measured in ARPES shown in figure 4 at 90 eV shows the locations in k-space of the final state, rather than the initial state Fermi surface.

When the crystal azimuth is rotated by 45° so that the vector potential **A** lies along the [110], the angular distributions change from those in figure 4, to those shown in figure 6.

The 45 eV pattern becomes a 3-sided rectangular box with the left side most intense and the right side barely visible. Since both even and odd d-e_g and d-t_{2g} states contribute, and neither have significant weight in the central horizontal plane (the plane of incidence), little can be said of the origin of the disappearance of the right side of the 'box' other than the matrix elements are small.

In the case of the 90 eV pattern, the 'X' becomes a vertical '|' rather than a '+'. Since the vector potential is lying within a mirror plane, the symmetry of this state must be odd, since photoemission intensity from it vanishes, and this is consistent with the structure at 90 eV originating from d-$t_{2g} \rightarrow f$ transitions.

Note that the considerations presented here *only include effects due to variations in the bulk matrix elements* and do not include the other effects that are well known to modify these angular distributions such as the surface effect, multiple-scattering, or forward-scattering effects that potentially appear for higher kinetic energies.

Other systems have been found to present photoemission angular distributions that reflect the symmetry of the final state, more than the initial Fermi surface contour as well. This observation of photoemission intensity contours and agree well with the final state k-space dispersion has also been reported for fcc Co films grown on Cu(100) [23]. In that case, shown in figure 7, even low photon energies between 21 and 45 eV gave ARPES patterns that were more representative of the final state $4p$ dispersion rather than the initial state $3d$ structure at the Fermi surface.

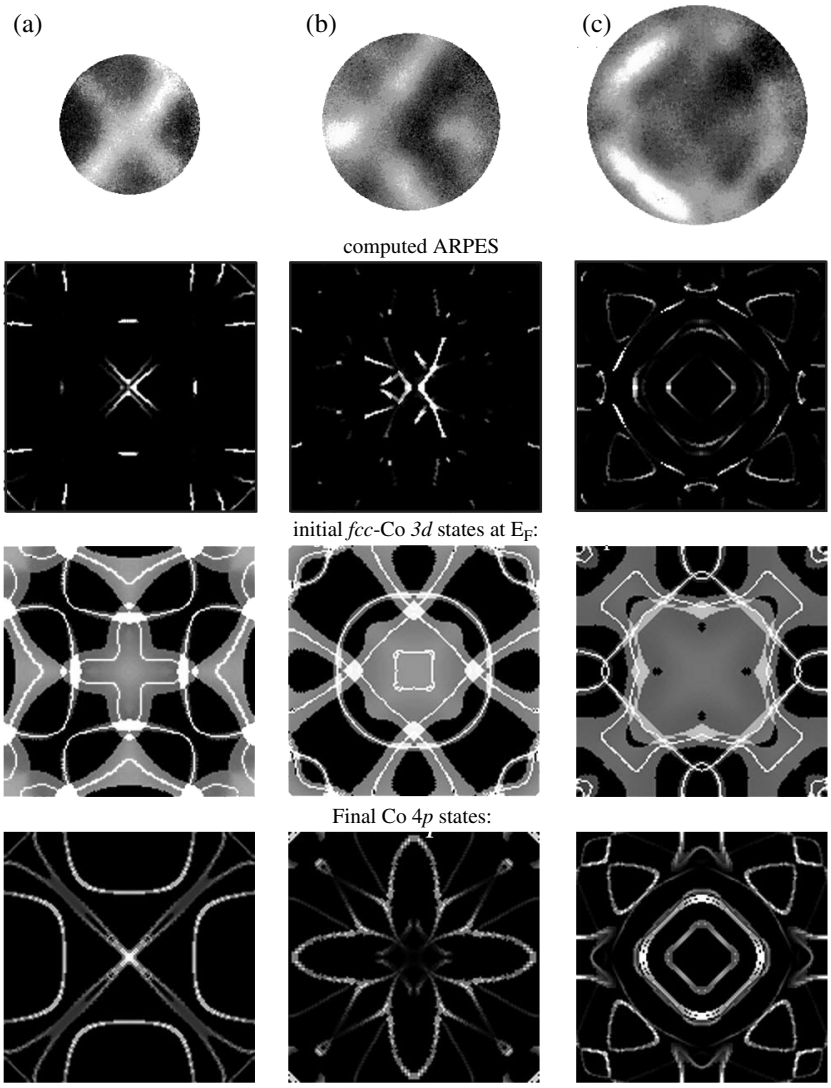

Figure 7. ARPES from 10 ML fcc Co/Cu(100) at $h\nu = 21$, 31, and 45 eV, columns (a)–(c). The ARPES patterns, scaled to uniform $k_\parallel$ are at the top, the computed ARPES below, followed by the DOS contours of the initial and final states. The ARPES patterns most closely resemble the final state contours. In this figure, darker computed contours are more intense.

Shown in figure 7 are the angular distributions from the Fermi surface of 10 ML fcc Co on Cu(100) at $h\nu = 21$, 31, and 45 eV, (a)–(c), along with the computed ARPES, the Co initial $3d$, and $4p$ final states. In the computations presented there, the initial and final states are considered within a ± 0.25 eV window so that the ARPES contours are computed with a final state lifetime that is small, resulting in narrow angular distributions. Nevertheless, it is clear that the computed angular distributions match the data reasonably well and yet do not reflect the density-of-states dispersion at the Fermi surface. Rather, they again reflect the structure of the final state. Again, considerations of additional phenomena that can also modify the angular distributions may provide better agreement with the observations, but the essential

physics involved in the polarization-dependent matrix elements provides a reasonably good basic explanation for the observed structures.

4.2. When are the matrix elements important?

As we have discussed above, extracting a Fermi surface contour from a thin film or from a single crystal using photoemission is an exercise that requires a close coupling to a computational description of the photoemission process. Many phenomena, both intrinsic and extrinsic, have been reported that modify the photoemission contours measured from the Fermi surface but we conclude that the most important first consideration must be the matrix elements that arise from a specific experimental geometry. This experimental geometry includes a combination of the electron emission/detection angles relative to the crystalline orientation as well as the incident photon polarization direction.

Since the photoemission matrix element is a coupling between the initial state, the Fermi surface, and the final state, a time-reversed LEED state, it will exhibit properties of both of these states, and each will contribute to the resulting transition probability. In regions of the Brillouin zone where either of these states have gaps, transitions cannot occur. This does not mean that intensity is not observed at these angles or photon energies since extrinsic effects such as final state diffraction or umklapp can add intensity from a transition in a different region of the Brillouin zone.

This is where computational support in interpreting angular distributions is invaluable. By evaluating regions that are gapped, and computing transition probability in regions that are not, one can better understand the origin of the measured angular distributions. Gaps can and do occur in the k-space distribution of both the initial state and the final state. This means that a photoemission contour does not necessarily reflect the shape of the Fermi surface, if that is the state being studied. In addition the symmetries of the initial and final states must be compatible, and give non-zero matrix elements.

At $h\nu = 45$ eV, photoemission from the top of the $3d$ electron bands of Cu give angular distributions that can be mapped directly back to the k-space contours of these bands. Although the polarization dependence modifies the intensities, the contours are well represented by the initial states. When the photon energy is increased to 90 eV, the angular distributions look completely unlike the initial state k-space contours and reflect the shape of the final state reached in the excitation. For this excitation, the symmetry of the states involved give zeros in the matrix elements when the polarization and emission angles are in the [011] azimuth.

In the thin film data presented, the monolayer of Ni on Cu gives angular distributions and polarization dependences from the Fermi surface like that for the Cu 3d bands at -2 eV. Although calculations for the monolayer are not yet available, this is presumably due to the similar nature of the electronic structures, differing by the 1-e reduced band filling of Ni.

Photoemission from the Fermi surface of Co thin films has been reported as well and those angular distributions follow the k-space contours of the final state, looking completely unlike the contours of the initial state Fermi surface.

5. Summary

Photoemission is a powerful tool for extracting information on the Fermi surfaces of a wide range of materials, and yet even a qualitative interpretation of photoemission data is not necessarily a simple matter. We have shown cases where the data can be directly related to Fermi surface contours within a bulk Brillouin zone, but we have also shown that observed contours may not always reflect the Fermi surface. Since photoemission is a method that relies

on a transition from an initial state (the Fermi surface) to a final state that is detected at a spectrometer, it is possible that the intensity contour that is measured reflects the structure of the final state. Without an accompanying computational model for the transition, it is not possible to be certain of the origin of the observed contours of intensity, but it is useful to suggest the types of electronic structures, and the photon energies where one could expect photoemission to provide data that follow the k-space distribution of the Fermi surface.

We note that photoemission transitions that produce intensity contours that do not resemble the Fermi surface, and give structure resembling the *final* state, exhibit some specific general features. First, the initial states in these transitions are relatively non-dispersive in energy, and have a wide k-space distribution as shown in figure 5. The final states, on the other hand involve states that disperse in energy more rapidly and most importantly have a narrower k-space distribution. When the transition occurs, the narrower k-space determined by the final state produces transitions localized in that part of the Brillouin zone. The k-space overlap of the initial and final states gives rise to structures that reflect the rapidly changing final state structure.

One might consider whether location within the Brillouin zone could affect the likelihood of an angular distribution better matching the initial state, for example when the photon energy samples states near Γ versus photon energies that sample states near a zone boundary near normal emission. The Cu and Ni data would suggest that it may be more common to see final state structure near the zone boundary but the Co data presented show that this can happen throughout the Brillouin zone. It is also important to recognize that the cases discussed here involve the relatively non-dispersive 3d electron Fermi surfaces. The sp-like Fermi surfaces of simpler metals such as Cu, with their more rapid dispersion, tend to give intensity contours that better reflect the initial state, albeit with strong polarization dependences of the matrix elements and resulting intensities.

Our final conclusion is that photoemission is a powerful tool for extracting electronic structures and Fermi surfaces but that a complete interpretation must involve a close coupling with computational models of the expected angular distributions for the specific experimental geometry employed.

Acknowledgments

We are pleased to acknowledge NSF funding for GJM under grant number NSF-02-13985 and RLK under DMR-0504654 and CHE-0615606.

References

[1] Himpsel F J 1983 Angle-resolved measurements of the photoemission of electrons in the study of solids *Adv. Phys.* **32** 1

[2] Plummer E W and Eberhardt W 1982 Angle-resolved photoemission as a tool for the study of surfaces *Adv. Chem. Phys.* **49** 533

[3] Strocov V N 2003 Intrinsic accuracy in 3-dimensional photoemission band mapping *J. Electron Spectrosc. Relat. Phenom.* **130** 65

[4] Knapp J A, Himpsel F J and Eastman D E 1979 Experimental energy band dispersions and lifetimes for valence and conduction bands of copper using angle-resolved photoemission *Phys. Rev.* B **19** 4952

[5] Gerlach A *et al* 2001 Lifetime of d holes at Cu surfaces: theory and experiment *Phys. Rev.* B **64** 085423

[6] Mankey G J *et al* 1997 Observation of a bulklike Fermi surface for a monolayer of Ni on Cu(001) *Phys. Rev. Lett.* **78** 1146

[7] Strocov V N, Starnberg H I and Nilsson P O 1997 Excited-state bands of Cu determined by VLEED band fitting and their implications for photoemission *Phys. Rev.* B **56** 1717

[8] Strocov V N, Claessen R and Blaha P 2003 Origin of photoemission final-state effects in $Bi_2Sr_2CaCu_2O_8$ by very-low-energy electron diffraction *Phys. Rev.* B **68** 144509
[9] Strocov V N *et al* 2001 Three-dimensional band mapping by angle-dependent very-low-energy electron diffraction and photoemission: methodology and application to Cu *Phys. Rev.* B **63** 205108
[10] Jensen E and Plummer E W 1985 Experimental band structure of Na *Phys. Rev. Lett.* **55** 1912
[11] Strocov V N, Finteis Th, Claessen R, Nicolay G, Ehm D, Colbus Y, Hüfner S, Starnberg H and Eyert Y 1997 BESSY Annual Report p 219
[12] Bansil A and Lindroos M 1998 Matrix element effects in the angle-resolved photoemission spectrum of BISCO *J. Phys. Chem. Solids* **59** 1879
[13] Bansil A *et al* 2002 First principles simulations of energy and polarization dependent angle-resolved photoemission spectra of Bi2212 *J. Phys. Chem. Solids* **63** 2175
[14] Sahrakorpi S, Lindroos M and Bansil A 2003 Site-selectivity properties of the angle-resolved photoemission matrix element in $Bi_2Sr_2CaCu_2O_8$ *Phys. Rev.* B **68** 054522
[15] Aebi P *et al* 1998 Angle-scanned photoemission: Fermi surface mapping and structural determination *Surf. Sci.* **404** 614
[16] Morikawa E *et al* 1992 Design of soft x-ray plane-grating monochromator for CAMD *Rev. Sci. Instrum.* **63** 1300
[17] Stockbauer R and Pararas A 1988 EMA construction *Nucl. Instrum. Methods Phys. Res.* A **266** 560
[18] Kurtz R L *et al* 1992 Photoelectron imaging of Fermi surfaces *Nucl. Instrum. Methods Phys. Res.* A **319** 257
[19] Blaha P *et al* 2001 WIEN2k, an augmented plane wave plus local orbitals program for calculating crystal properties (Vienna University of Technology, Austria)
[20] Perdew J P, Burke K and Ernzerhof M 1996 Generalized gradient approximation made simple *Phys. Rev. Lett.* **77** 3865
[21] Fuster G *et al* 1990 Electronic-structure and related properties of silver *Phys. Rev.* B **42** 7322
[22] Janak J F, Williams A R and Moruzzi V L 1975 Self-consistent band theory of the Fermi-surface, optical, and photoemission properties of copper *Phys. Rev.* B **11** 1522
[23] Gao X *et al* 2003 Dominance of the final state in photoemission mapping of the Fermi surface of Co/Cu(001) *Phys. Rev. Lett.* **90** 037603